

pubs.acs.org/acscatalysis Research Article

# Hydrogen Adsorption at the Au/TiO<sub>2</sub> Interface: Quantitative Determination and Spectroscopic Signature of the Reactive Interface Hydroxyl Groups at the Active Site

Akbar Mahdavi-Shakib, Lauren C. Rich, Todd N. Whittaker, and Bert D. Chandler\*



Cite This: ACS Catal. 2021, 11, 15194–15202



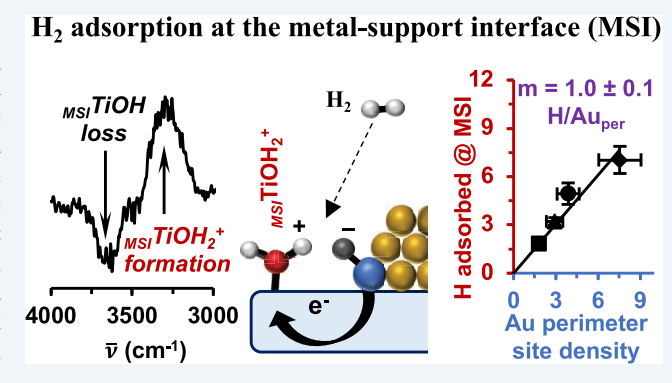
**ACCESS** 

III Metrics & More



Supporting Information

ABSTRACT: Infrared spectroscopy shows that  $H_2$  adsorbs heterolytically at the metal—support interface (MSI) of  $Au/TiO_2$  catalysts. This generates stable protonated MSI hydroxyls, which are chemically distinct from adsorbed water and free surface hydroxyls. IR spectra collected during  $H_2$  adsorption revealed changes associated with the loss of unprotonated interface hydroxyls ( $_{\rm MSI}$ TiOH) and the appearance of protonated interface hydroxyls ( $_{\rm MSI}$ TiOH $_2^+$ ). This allowed us to identify a spectroscopic signature associated with MSI hydroxyls interacting with Au nanoparticles and separate that signature from the unmodified hydroxyls that dominate the surface. Prior to  $H_2$  adsorption, MSI hydroxyls are electron-rich relative to other surface hydroxyls on the catalyst. As a consequence, MSI hydroxyls are more basic,



which likely contribute to their involvement in  $H_2$  activation. The surface density of the  $_{\rm MSI}{\rm TiOH_2}^+$  species was quantified with the broad-background absorbance (BBA) associated with electron injection into the support during  $H_2$  adsorption. Quantifying these signals across a series of catalysts showed that each Au perimeter atom is associated with one reactive  $_{\rm MSI}{\rm TiOH}$  group. This unexpected result indicates that Au modifies the local structural and electronic properties of the support. Thus, the synergism between Au and  ${\rm TiO_2}$  produces electron-deficient Au particles, which are stronger Lewis acids, and increases the number of electron-rich MSI hydroxyls, which are stronger Brønsted bases.

**KEYWORDS:** gold catalyst,  $H_2$  adsorption, metal—support interface, broad-background absorbance, titania, FTIR spectroscopy, surface hydroxyls, catalyst active site

### ■ INTRODUCTION

Supported metal catalysts, typically consisting of a metal nanoparticle (NP) immobilized on an oxide support, are one of the most important classes of industrial catalysts. Their catalytic activity and selectivity are ultimately controlled by the chemistry at the catalytic active site, yet the nonuniformity of these materials presents considerable challenges to identifying and characterizing the active sites(s) for a particular reaction. This is especially true for reactions where the interface between the metal NP and the support is a key contributor to the catalytic chemistry. Important industrial examples of these reactions include CO<sub>2</sub> hydrogenation, methanol synthesis, biomass upgrading, CO oxidation, the water gas shift reaction, introarene hydrogenation, and electrocatalytic energy conversion.

The metal—support interface (MSI) sites are typically associated with <5% of the total number of metal atoms in a catalyst and an even smaller fraction of the support surface. This makes the MSI sites particularly difficult to interrogate. The relatively low activity of Au surfaces, however, makes supported Au catalysts ideal materials for probing MSI

chemistry. Since Haruta's seminal discovery of low-temperature CO oxidation activity over supported Au nanoparticles, <sup>20</sup> Au catalysts have been investigated for a variety of organic oxidations, <sup>21–24</sup> oxidative couplings, <sup>25,26</sup> and other nonaerobic processes. <sup>27</sup> Various chemistries at the MSI are featured prominently in these reactions. <sup>21,28–32</sup> The combination of the support Brønsted acid—base chemistry with metal surface redox chemistry is a similarly broad theme that extends to other important catalytic systems as well. <sup>33–35</sup>

Even though Au catalysts often have highly desirable selectivity for important industrial reactions, Au-catalyzed hydrogenations have garnered less attention than well studied oxidations. Some examples include semihydrogenations, <sup>36–43</sup>

Received: September 25, 2021 Revised: November 19, 2021 Published: December 7, 2021





Table 1. Catalyst Characterization Data

catalyst	% Au	surface area $\left(m^2/g\right)$	$d_{ave}(Au)^a (nm)$	per density $^b$ ( $\mu$ mol Au $_{per}$ /g cat.)	BBA calibration <sup>c</sup> (mmol H/mol Au/AU)
a	$1.0 \pm 0.1$	$48 \pm 3$	$2.7 \pm 0.9$	$1.8 \pm 0.3$	$3.0 \pm 0.3$
ь	$2.3 \pm 0.2$	$48 \pm 3$	$3.0 \pm 1.0$	$2.9 \pm 0.6$	$4.6 \pm 0.1$
c	$4.5 \pm 0.4$	$48 \pm 3$	$2.9 \pm 0.8$	$7.5 \pm 1.4$	$1.4 \pm 0.1$
d	$4.5 \pm 0.4$	$31 \pm 3$	$4.2 \pm 1.2$	$3.9 \pm 0.7$	$1.2 \pm 0.1$

<sup>a</sup>See Figure S1 for STEM images. <sup>b</sup>Determined from particle size analysis of STEM images; details in the SI. <sup>c</sup>See Figure S9 for calibration curves.

selective hydrogenations, 44,45 nitro-aromatic reduction, 17,46,47 hydrodechlorination, 48 and biomass conversion. 49–52 The primary reason these reactions have not been employed industrially is the well-known low hydrogenation activity of Au, which is orders of magnitude lower than Pt, Pd, or Ni. At the same time, this presents an important opportunity: if the fundamental hydrogenation chemistry can be understood and improved, there are numerous potential applications for Au selective hydrogenation catalysts.

There is now broad evidence that fast  $H_2$  activation over Au occurs via heterolytic H–H activation at the MSI. Inelastic neutron scattering and Fourier transform infrared spectroscopy (FTIR) experiments provided clear spectroscopic evidence for both Au–H and protons on the support after  $H_2$  adsorption. Rossi's group has also shown that Au-catalyzed hydrogenations are considerably faster in the presence of a base. Our own work has provided an abundance of kinetic evidence for the importance of heterolytic  $H_2$  activation in hydrogenation reactions and allowed us to quantify  $H_2$  adsorption with in situ FTIR spectroscopy.

Important fundamental questions remain regarding the nature of the  $\rm H_2$  activation active site(s) and how they might be modified to improve broader hydrogenation activity. Particle size effects have been implicated in several high-profile Au-catalyzed reactions  $^{21,23,31,58-61}$  and have been suggested to be important in selective hydrogenations. He article size effects can have both structural and electronic origins but it is difficult to sort out their relative importance in a given reaction. Lear determinations of the number of active sites and spectroscopic signatures that enable monitoring electronic modifications are necessary to understand the relative impact of structural and electronic effects, and hence, improve catalytic activity.

While it is clear that the details of the Au-support contact structure are key contributors to the unique catalytic chemistry of Au, a few quantitative measures for examining these details are available.  $^{62}$  We previously showed that  $H_2$  adsorption on Au/TiO<sub>2</sub> results in electron injection into the support; this can be quantified via a broad-background absorbance (BBA) and correlated with volumetric adsorption measurements.<sup>57</sup> In this work, we extend our study to include a full examination of the support hydroxyls directly at the interface. These hydroxyls have very low surface concentrations, making them exceptionally difficult to probe and characterize. Using a series of Au/ TiO<sub>2</sub> catalysts, we report and quantify clear spectroscopic signatures associated with (i) the proton transfer to MSI hydroxyls and (ii) the corresponding "loss" of unprotonated hydroxyls. Tracking this signature across the catalysts and quantifying the number of adsorbed H2 molecules as a function of the catalyst perimeter site density revealed new information regarding the nature and number of H<sub>2</sub> adsorption sites.

# ■ RESULTS AND DISCUSSION

Catalysts. We studied H<sub>2</sub> adsorption on a series of four Au/TiO<sub>2</sub> catalysts using FTIR spectroscopy and volumetric

adsorption experiments. The catalysts were prepared with the goal of varying the density of Au—TiO<sub>2</sub> perimeter sites. The details on catalyst synthesis and characterization, as well as scanning transmission electron microscopy (STEM) images, are available in the SI; these methods and results are comparable to what we have described previously. ST Selected characterization data (particle sizes, elemental analysis, BET surface areas, and H<sub>2</sub> adsorption measurements) are available in Table 1. Three catalysts (a—c) were prepared with similar average particle sizes (2.7—3.0 nm) but with different Au loadings. A fourth catalyst (d) was reduced at a moderately higher temperature, yielding slightly larger (4.2 nm) particles. The perimeter site density for each catalyst was determined by summing the contributions of each statistical bin in the full particle size distribution histogram (see the SI).

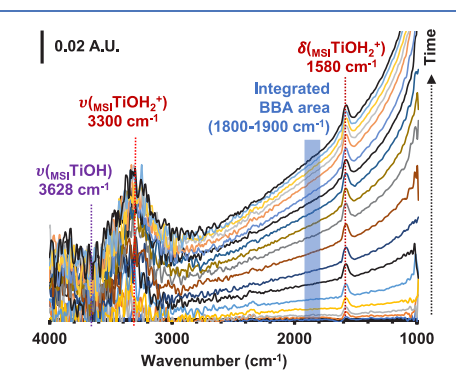


**Figure 1.** FTIR study of  $H_2$  adsorption on Au/TiO $_2$  as a function of time. The spectra shown are difference spectra recorded after exposure of catalyst b to 40%  $H_2$  in  $N_2$  at 60 °C. Spectra are referenced to the single-beam spectrum of the sample recorded immediately before exposure to  $H_2$ . The blue bar shows the integrated area used for quantifying the BBA signal. FTIR spectra for all four catalysts are provided in Figure S3. The AU unit stands for absorbance units.

# Spectroscopic Evidence for H<sub>2</sub> Adsorption at the MSI.

Figure 1 shows representative difference FTIR spectra collected during  $H_2$  adsorption on a freshly reduced 2.3%  $Au/TiO_2$  catalyst (catalyst b); spectra for all four catalysts are provided in Figure S3. Briefly, the change in light transmission over the entire spectrum, which we describe as a broadbackground absorbance (BBA), is characteristic of electron transfer into the conduction band of  $TiO_2$ .  $^{31,57,64-67}$  When correlated with volumetric  $H_2$  adsorption measurements, the BBA signal can be used to quantify  $H_2$  adsorption on  $Au/TiO_2$  catalysts.  $^{57}$  A new feature centered near 1580 cm $^{-1}$ , which we previously assigned to the  $\delta_{HOH}$  vibration of protonated MSI hydroxyl groups ( $_{MSI}TiOH_2^+$ ), also appears. These features occur during  $H_2$  adsorption on all four catalysts, as shown in Figure S3. Control experiments on comparably pretreated P-25 titania showed no  $H_2$  uptake in volumetric adsorption

experiments and no changes in the IR spectrum upon the addition of H<sub>2</sub>.

The appearance of protonated MSI hydroxyl groups and concomitant electron transfer to the support, evidenced by the BBA signal, indicates H<sub>2</sub> adsorption results in the net transfer of a proton-electron pair to the support. We refer to this proton-electron pair as a hydrogen atom equivalent (HAE) to distinguish it from a pure proton or a true H-atom, which describes a proton strongly coupled to an electron with a 1s orbital ground state. Thus, transferring the HAE onto the support captures the following process

$$_{MSI}$$
TiOH + HAE  $\rightleftharpoons$   $_{MSI}$ TiOH<sub>2</sub><sup>+</sup> + e<sup>-</sup>(TiO<sub>2</sub>) (1)

where MSITiOH represents the active perimeter hydroxyls, MSITiOH<sub>2</sub><sup>+</sup> represents the protonated active perimeter hydroxyls, and e<sup>-</sup>(TiO<sub>2</sub>) represents the added electron to the support observable as BBA. DFT calculations indicate that the electron is broadly delocalized across the support surface, with roughly one-half of an electron localized on the protonated Ti–OH group. <sup>54</sup> For simplicity, we treat both the proton and electron as separate entities.

DFT calculations in support of kinetics measurements indicate that the adsorbed proton and electron are tightly coupled, even though the electron is broadly delocalized. We previously characterized the HAE as a "waterlike species" based on the  $\delta_{\rm HOH}$  vibrational frequency; however, we do not believe that the bulk of the data is consistent with the adsorbed water. While protons and deuterons are readily exchanged, we see no evidence that the O species are removed, even at 150 °C under  $\rm H_2$  or under flowing  $\rm N_2$  during  $\rm H_2$  desorption. Additionally, we can conceptualize a process by which a proton is transferred to a hydroxyl group with a formal negative charge, while a partial negative charge is transferred to a Ti–O antibonding state, polarizing the Ti–OH bond to localize greater charge on the O atom.  $^{54}$ 

While the transfer of a proton to a hydroxyl group certainly results in a waterlike species, it is then unclear how that water would become partially oxidized when the electron density is transferred to a Ti–O or a Ti-based state. In fact, our DFT calculations show the opposite, with the protonated hydroxyl removing the electron density from the surface. Therefore, while the best description of the surface species likely lies somewhere in between a "waterlike species" and a "protonated hydroxyl", we presently believe that the "protonated hydroxyl" (MSITiOH<sub>2</sub><sup>+</sup>) description is more consistent with the observed and modeled chemistry.

Our previous study focused on quantifying the BBA signal and included only a cursory examination of changes to the MSI hydroxyls on two catalysts; <sup>57</sup> the extension of this study to four catalysts allows for a more complete examination of the hydroxyl groups involved in H<sub>2</sub> activation. Upon H<sub>2</sub> adsorption, an additional feature near 3300 cm<sup>-1</sup> appears, corresponding to a new O–H stretching frequency. A close inspection of the spectra reveals that the growth of the 3300 cm<sup>-1</sup> band coincides with a feature associated with the loss of absorbance at ~3628 cm<sup>-1</sup> (Figure 2A). Similar features are observed for all four catalysts; see Figure S3. We therefore assign the 3628 and 3300 cm<sup>-1</sup> bands to MSITiOH and MSITiOH<sub>2</sub><sup>+</sup> stretching vibrations, respectively.

Figure 2B shows the plots of the  $_{MSI}$ TiOH and  $_{MSI}$ TiOH $_2^+$  stretching band peak areas vs the peak area associated with the  $_{MSI}$ TiOH $_2^+$  scissoring band ( $\delta_{HOH}$ ) for four different Au/TiO $_2$ 

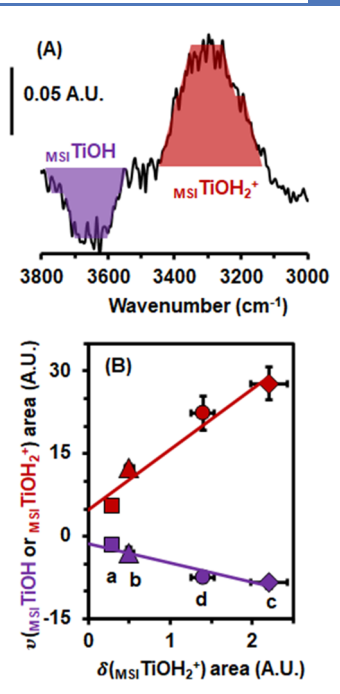


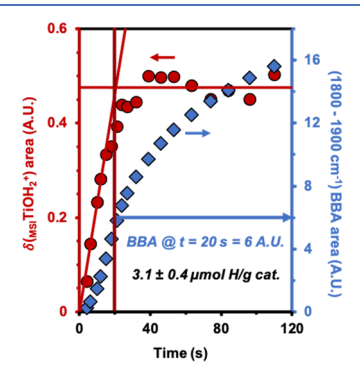
Figure 2. (A) FTIR difference spectrum of catalyst c under 40%  $\rm H_2/N_2$  at 70 °C. The spectrum is referenced to the single-beam spectrum of the sample recorded immediately before exposure to  $\rm H_2$ . The negative absorbance feature (highlighted in purple) shows the species consumed during  $\rm H_2$  adsorption; the positive absorbance feature (highlighted in red) shows species generated during  $\rm H_2$  adsorption. The BBA feature was subtracted for clarity. (B) Integrated areas of the negative  $_{\rm MSI}$ TiOH stretching band (purple) and the positive  $_{\rm MSI}$ TiOH $_2$ + stretching band (red) as a function of the  $_{\rm MSI}$ TiOH $_2$ + scissoring band centered at 1580 cm $^{-1}$  (not shown). Full spectra are available in Figure S3. The reported peak areas are averages of the extracted areas from 5 to 10 spectra of the saturated MSI sites (see Figure 3); error bars indicate the corresponding standard deviations. Letters a, b, c, and d represent catalysts a, b, c, and d, respectively (see Table 1).

catalysts. The changes to these peak areas are linearly correlated, indicating that each  $_{\rm MSI}{\rm TiOH}$  hydroxyl "lost" during  $\rm H_2$  adsorption is converted to  $_{\rm MSI}{\rm TiOH_2}^+$  (Figure 2B). Differences in the slopes of the lines are attributed to differences in extinction coefficients for various vibrational modes. With these linear correlations, observed changes to  $_{\rm MSI}{\rm TiOH_2}^+$ , which are more easily quantified, must be proportional to the number of active hydroxyls. This internal consistency is a prerequisite for evaluating the number of active hydroxyl groups across all of the catalysts. Our results also showed that the intensity of all three  $\nu(_{\rm MSI}{\rm TiOH})$ ,  $\nu-(_{\rm MSI}{\rm TiOH_2}^+)$ , and  $\delta(_{\rm MSI}{\rm TiOH_2}^+)$  bands are directly proportional to the perimeter density of the catalysts (Figure S4), indicating that these species are specific to the MSI of Au/ TiO<sub>2</sub> catalysts.

We have not found evidence for a Au–H band in any of our studies. While some have attributed bands around 2130 cm<sup>-1</sup> to Au–H, <sup>53,68</sup> we and others <sup>66,69</sup> have not been able to observe this for Au/TiO<sub>2</sub>. DFT calculations indicate that Au–H species are unstable relative to deprotonation by TiO<sub>2</sub>. <sup>54</sup> Hence, either the extinction coefficient for Au–H is too low for us to observe or the lifetime of Au–H species appears to be too short to be observed in our FTIR experiments. Given the relative stability of MSITiOH<sub>2</sub><sup>+</sup>, we favor the latter explanation. Thus, at least over the timescale of our experiments, H<sub>2</sub>

adsorption on  ${\rm Au/TiO_2}$  catalysts is best described as the addition of two HAEs to the MSI.

Quantification of Active Hydroxyls via FTIR Titration. Since H<sub>2</sub> adsorption involves both Au atoms and <sub>MSI</sub>TiOH sites, the number of active sites cannot be determined simply from the number of perimeter sites on Au nanoparticles (Au<sub>ner</sub>). 38-40,53-57 The local structure of the support around Au particles must also play a role, as active sites require hydroxyl groups that are (i) physically close enough to Auper for H<sub>2</sub> to bridge the two components of the site and (ii) sufficiently basic to accept a proton during H2 activation. The surface terminations of anatase and rutile structures typically have a combination of terminal (basic) and bridging (acidic) hydroxyls. Using this as a guide, there is no a priori reason to expect that every Ti-OH next to a Auper atom will meet both of the criteria necessary for an active site; rather, the expectation should be that roughly one-half of surface hydroxyls near Au particles will be sufficiently basic to activate H<sub>2</sub>. We examined this more carefully by developing a systematic method for estimating the number of active hydroxyls at the MSI based only on the IR data, which is a measure of the number of active sites independent of the Au



particle size information from TEM data.

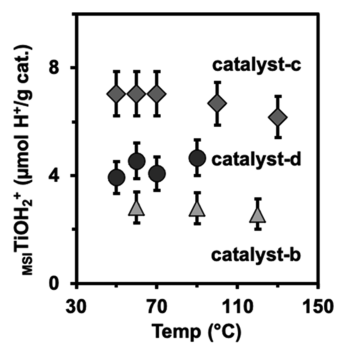
Figure 3. FTIR titration method for determining the quantity of adsorbed H at  $_{\rm MSI}{\rm TiOH_2}^+$  saturation. Changes to the BBA and  $_{\rm MSI}{\rm TiOH_2}^+$   $\delta_{\rm HOH}$  band profiles during H<sub>2</sub> adsorption on catalyst b (60 °C, 40% H<sub>2</sub>/N<sub>2</sub>; spectra in Figure 1) are shown. The BBA intensity was monitored by measuring the area under the spectrum between 1800 and 1900 cm<sup>-1</sup> (blue bar in Figure 1). The  $_{\rm MSI}{\rm TiOH_2}^+$  saturation time is determined from the intersection of linear fits to the early time increase regime and the flat portion of the  $\delta(_{\rm MSI}{\rm TiOH_2}^+)$  profile. Note: while the plots only show the early portion of the experiment, all of the saturated data (~1000 s) was used to fit the flat line (Figure S10).

Figure 3 shows the integrated areas of the BBA and MSITiOH<sub>2</sub><sup>+</sup> signals for the spectra presented in Figure 1 as a function of time. The MSITiOH<sub>2</sub><sup>+</sup> band stabilizes in about 30 s, which marks the point at which MSITiOH sites become saturated with protons. While this correlation is clear, the extinction coefficients of MSITiOH and MSITiOH<sub>2</sub><sup>+</sup> bands are unknown; consequently, the intensity of these vibrational features cannot be directly used to extract the number of active hydroxyls.

The calibrated BBA signal is linearly related to the total quantity of adsorbed H and can be used to evaluate the amount of  $\rm H_2$  adsorbed on the catalyst (e.g., HAEs) when  $\rm _{MSI}TiOH_2^+$  signal becomes saturated. BBA calibration plots for

each catalyst are available in the SI (Figure S9); the extracted calibration factors are reported in Table 1. The  $_{\rm MSI}$ TiOH $_2^+$  saturation time is determined from the intersection of linear fits to the early time increase regime and the flat portion of the  $\delta_{\rm HOH}$  profile. Determining the amount of hydrogen (HAE) required to saturate the  $_{\rm MSI}$ TiOH $_2^+$   $\delta_{\rm HOH}$  band provides a quantitative spectroscopic determination of the number of active MSI hydroxyls. We refer to this systematic method as FTIR titration. In this titration, the hydroxyl IR absorption area (bending or stretching vibration) is linearly correlated with the BBA signal. The BBA signal for each sample is calibrated to volumetric H $_2$  adsorption measurements as we have described previously. S7

Thus, the FTIR titration provides a direct quantitative measure of the number of reactive interface hydroxyls. While several TEM studies have shed light onto  ${\rm Au-TiO_2~MSI,^{70-72}}$  this information is not available via TEM due to three fundamental limitations: (i) TEM is limited by sample bias, as Au particles are most easily imaged on the thinnest sections of the support; (ii) TEM is limited to the analysis of a very small number of particles. Even 10 000 particles is a miniscule fraction of what is present on 1 mg of catalyst; and (iii) TEM cannot directly probe hydroxyl reactivity. Thus, while excellent TEM images may be able to show that there is one hydroxyl group per Au, TEM cannot indicate if all of those hydroxyls are reactive. The FTIR titration provides exactly that information and samples orders of magnitude more particles than is possible with TEM.



**Figure 4.** Extracted number of active perimeter hydroxyls for catalysts b, c, and d as a function of temperature using FTIR titration.

Using the data in Figure 3 as an example, the extracted quantity of  $3.1 \pm 0.4~\mu \text{mol}$  H/g is then interpreted as the number of active perimeter hydroxyls for catalyst b. We performed this titration at several different adsorption temperatures. The extracted number of active perimeter hydroxyls as a function of temperature is shown in Figure 4. For any given catalyst, the extracted values are essentially constant for analysis temperatures up to about 100 °C. Above that temperature, there may be a slight decline in the number of saturated perimeter sites. This is not surprising as eventually equilibrium considerations will require higher H<sub>2</sub> pressures to overcome entropy and continue saturating the MSI hydroxyl group.

Figure 4 presents the MSI TiOH<sub>2</sub><sup>+</sup> density in terms of sites per gram of catalyst, and so the observed differences between the catalysts are expected based on different Au weight loadings. A plot of the same data normalized to the perimeter site density is available in the SI (Figure S11B). The relationship trend is readily visualized by plotting the extracted number of active

ACS Catalysis pubs.acs.org/acscatalysis Research Article

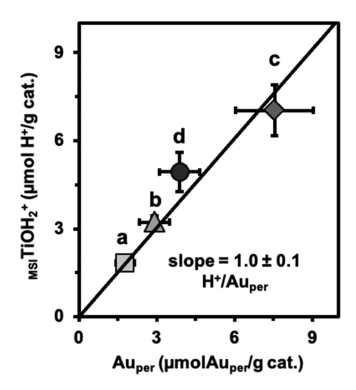


Figure 5.  $H_2$  adsorbed at  $_{\rm MSI}$ TiO $H_2^+$  saturation (FTIR titration) as a function of the catalyst perimeter site density (STEM image analysis). The *y*-axis values were determined at 70 °C, except catalyst b, which was determined at 60 °C. The slope of the fitted line shows  $H^+/Au_{\rm per}$  at  $_{\rm MSI}$ TiO $H_2^+$  saturation. The uncertainty in the slope was determined using the regression analysis of the linear fit. The letters a, b, c, and d next to the symbols represent catalysts a, b, c, and d, respectively (see Table 1).

hydroxyl groups (IR and volumetric adsorption data) against the number of  $Au_{per}$  sites (STEM image analysis), as shown in Figure 5. This is essentially a bulk determination of the number of active sites on the catalyst that simultaneously provides information on (i) the number of adsorption sites and (ii) the structural stoichiometry of active site components. The bulk determination of the number of active sites on Au catalysts for any reaction, much less hydrogenation, has not previously been possible.

The linear relationship with a slope of  $1.0 \pm 0.1$  H/Au<sub>per</sub> (Figure 5) indicates that, on average, one H<sup>+</sup> is transferred to a reactive MSI hydroxyl group for each Au<sub>per</sub> site. This 1:1 relationship implies that there is one basic OH per Au<sub>per</sub> atom. This relation holds for all of the catalysts within a very reasonable margin of error. It also covers a relatively large range of Au nanoparticle sizes—roughly from 1.5 to 7 nm, which is the particle size range of greatest interest for catalysis.

This is a somewhat unexpected finding, as structural models of anatase and rutile  ${\rm TiO_2}$  generally show a combination of both bridging (acidic) and terminal (basic) hydroxyl groups. <sup>73,74</sup> Given the spacing between surface hydroxyls on common  ${\rm TiO_2}$  surface terminations, Au atoms are not large enough to accommodate both bridging and terminal hydroxyls at every  ${\rm Au_{per}}$  site. The generation of one basic TiOH per  ${\rm Au_{per}}$  site therefore suggests a significant local modification of the support around Au nanoparticles. We note that this is not typically incorporated into computational models, which typically freeze the support surface termination to the bulk geometry to reduce computational expense.

We cannot rule out the possibility that the  $H_2$  activation activity correlates with the particle size due to activation on low-coordinate corner or edge sites followed by transfer to MSI sites; this would result in the same final state as we observe spectroscopically. The corner site density dependence on particle diameter  $(d^{-3})$  is almost indistinguishable from the perimeter site density dependence  $(d^{-2})$  over this particle size range, so a nearly equivalent correlation for Figure 5 can be prepared using the corner site density (further details available in the SI). Several factors make this less likely. First, previous DFT calculations indicate that homolytic  $H_2$  activation on low-coordination sites is thermodynamically uphill.  $^{54,56,66,75-78}$  Second, several well-conceived studies from the Rossi group

have clearly shown that  $H_2$  activation on Au nanoparticles is facile in the presence of basic amine groups; they report essentially no hydrogenation activity in the absence of the added amine. These amines can be added in solution with various diamines or via the support using N-doped carbon supports. Both in their systems and in ours, heterolytic  $H_2$  activation avoids the formal oxidation of Au (which is more electronegative than H) during homolytic dissociative chemisorption.

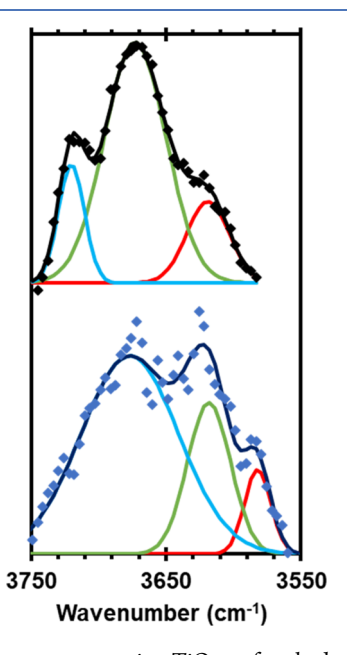


Figure 6. FTIR spectra comparing  $TiO_2$  surface hydroxyls (top) with changes observed during  $H_2$  adsorption (bottom). The top FTIR spectrum is of a dry  $Au/TiO_2$  catalyst (catalyst a), collected at 200 °C and referenced to KBr at 200 °C. The bottom spectrum shows the  $_{MSI}TiOH$  bands that undergo protonation upon  $H_2$  adsorption. The symbols in both top and the bottom panels show spectral data points, and the dark lines are the sum of three individual Gaussian curves (lighter lines). Spectra were offset for clarity. See Figures S16 and S17 for more details on the fitted Gaussian curves.

Electronic Modification of  $_{MSI}$ TiOH by Au. The observed 1:1 relationship between active perimeter hydroxyls and Au<sub>per</sub> sites prompted us to more carefully consider the spectroscopic signatures associated with each of the hydroxyl bands. Anatase surface hydroxyls typically show three  $\nu_{OH}$  stretches at 3718, 3673, and 3641 cm<sup>-1</sup>, while rutile surfaces typically have two bands at 3695 and 3660 cm<sup>-1</sup>. Figure 6 shows that a dried sample of catalyst a has TiOH  $\nu_{OH}$  bands centered at  $\sim$ 3673 cm<sup>-1</sup>. This spectrum is well described by a linear combination of three Gaussian curves centered at 3619, 3673, and 3720 cm<sup>-1</sup>; it is therefore consistent with the composition of P-25 titania, which is predominately anatase.

The negative peak centered at  $\sim 3628~{\rm cm}^{-1}$  in Figure 2A is associated with the loss of the  $v(_{\rm MSI}{\rm TiOH})$  stretch that can be regarded as the spectroscopic signature of MSI hydroxyls prior to  ${\rm H_2}$  adsorption. The low concentration of MSI hydroxyls, coupled with the high background absorbance of the sample at these wavelengths, adds considerable noise to these spectra. To facilitate comparison with unmodified hydroxyls on  ${\rm TiO_2}$  (Figure 6), we averaged four spectra collected when MSI hydroxyls are saturated (see Figure S17) and inverted the spectrum. The resulting spectrum is also well described by

three Gaussians centered at 3582, 3618, and 3677 cm<sup>-1</sup>. These values are, on average, ~45 cm<sup>-1</sup> red-shifted relative to anatase surface hydroxyls, indicating a substantial electronic perturbation of the support at the MSI. The differences in the relative sizes and distribution curves fitted to active hydroxyls are also consistent with structural changes at the MSI suggested above.

The observed lower stretching frequency indicates that active hydroxyls are characterized by weaker, less polar O-H bonds. It follows that less polar O-H bonds are associated with more electron-rich O atoms, so MSI hydroxyls are expected to be stronger bases than surface hydroxyls away from Au. A recent DFT study also suggested the net partial electron transfer from Au to TiO2 at the interface, consistent with this observation.<sup>70</sup> This conclusion is consistent with two related observations. First, interface hydroxyls remain protonated while H-D exchange occurs between mobile H+ and D+ on the support. 54 Second, H<sub>2</sub> adsorption continues after MSI sites are saturated (presumably due to a spillover-like mechanism), yet interface hydroxyls are always observed under H2. The MSITiOH2+ bands are the first to appear upon adsorption and the last to disappear during desorption; HAEs are clearly more stable at the MSI than elsewhere on the catalyst.<sup>54</sup> These results, along with the spectroscopic signature, are all consistent with the stronger Bronsted basicity of MSI hydroxyls.

The 3300 cm<sup>-1</sup>  $v(_{MSI}TiOH_2^+)$  stretch in the top spectrum of Figure 2 is  $\sim 330$  cm<sup>-1</sup> further red-shifted from  $v(_{MSI}TiOH)$ and is about 3 times more intense than the corresponding negative band of  $v(_{MSI}TiOH)$ . This red shift is too large and in the wrong direction to be attributed solely to the protonation of active hydroxyls. DFT calculations show that the vibrational frequency of isolated surface hydroxyls and isolated water molecules (e.g., without H-bonding) adsorbed on TiO<sub>2</sub> are almost indistinguishable.<sup>74</sup> A large red shift and a significant increase of the molar absorptivity are typical when functional groups are directly involved in H-bonding.80 Our results suggest that the MSITiOH species are largely isolated but the protonated MSI TiOH2+ species participate in H-bonding, either with near-by hydroxyls or with trace amounts of surface water. (Prior to H<sub>2</sub> adsorption, the surface is equilibrated with <1  $\mu$ bar of water that remains after purifying UHP gases with a dry ice/isopropanol bath.)

The  $\delta_{\text{HOH}}$  band for water is well known to be sensitive to its local environment,  $^{81-84}$  and it has been established that  $\delta_{\text{HOH}}$ bands blue-shift upon increasing the H-bonding strength.8 For example, the molecular water  $\delta_{\rm HOH}$  band ranges from 1650 cm<sup>-1</sup> for liquid water to 1590 cm<sup>-1</sup> for isolated gas-phase molecules. 82 Figure 7 compares  $\delta_{HOH}$  bands for the adsorbed water (H2O-Au/TiO2) and for the MSITiOH2+ species generated by H<sub>2</sub> adsorption (H<sub>2</sub>-Au/TiO<sub>2</sub>). The water band at 1620 cm<sup>-1</sup> indicates substantial H-bonding interactions. The  $\delta_{HOH}$  band for  $_{MSI}TiOH_{2}^{+}$  is red-shifted even further to 1580 cm<sup>-1</sup>, even though the  $v(_{MSI}TiOH_2^+)$  stretching frequency suggests that the MSITiOH2+ species participate in H-bonding. Direct interpretation of the bending vibration frequency is difficult, as charges associated with H+ and (partial) electron transfer to the MSITiOH are not clear. However, the low scissoring frequency cannot be attributed to H-bonding and therefore must have structural and/or electronic origins, making IR observations internally consistent, and consistent with a significant structural and electronic modification of the support by Au.

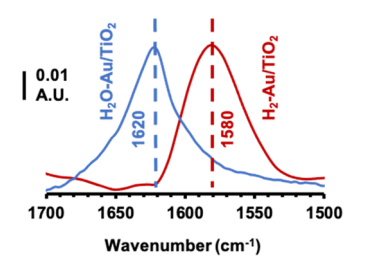


Figure 7. FTIR spectra of the  $\delta_{HOH}$  scissoring vibration of adsorbed water  $(H_2O-Au/TiO_2)$  and  $H_2$   $(H_2-Au/TiO_2)$  on  $Au/TiO_2$  in the scissoring region. Spectra are difference spectra referenced to the single beam of the sample before  $H_2$  or  $H_2O$  adsorption. Full spectra for  $H_2$  and  $H_2O$  adsorption are shown in Figures S3 and S13, respectively.

The Bond and Thompson model for CO oxidation over Au/ TiO<sub>2</sub> catalysts<sup>86</sup> originally postulated a unique interaction between Au and the interface Ti-OH groups. Although their suggestion that Au MSI atoms are fully oxidized to Au(I) likely overstates the degree of charge transfer, and perhaps, overly localizes the process on a small number of Au atoms, the broader suggestion of the important electronic interaction between the two components appears to be appropriate. Most recently, Fujitani et al. examined water TPD from single-crystal Au/TiO2 model catalysts, observing a high-temperature desorption peak whose intensity increases linearly with the Au perimeter site density.87 They attributed this unique water TPD feature to the presence of "special hydroxyls" that are selectively formed at the Au/TiO2 MSI. While our work is on high-surface-area materials, our results show a similar linear increase with the perimeter site density (see Figures 5 and S4), providing a complementary spectroscopic signature to their TPD identification. Further, our studies show that interface hydroxyls are directly involved in H<sub>2</sub> adsorption, and by extension, in Au-catalyzed hydrogenations and CO PrOx. 54,56,57,88

The unique spectroscopic signature of MSI hydroxyls above and Fujitani's report indicate an electronic influence of Au on MSI hydroxyls. Interactions with Au may also perturb the surface hydroxylation, effectively converting bridging hydroxyls at the MSI to terminal (basic) hydroxyls. Most of the stable surface terminations of anatase and rutile contain both bridging and terminal hydroxyls. However, a number of lowenergy pathways are available for the hydrolysis of bridging hydroxyls, 74 and small deviations from stoichiometry lead to the formation of crystallographic shear planes and surface roughening.<sup>89</sup> Even the rutile (110) surface, which is the most stable and most studied single-crystal surface, is not well understood because of structural changes due to sample pretreatment and sample history. 90 It is therefore not unreasonable to expect that interactions with Au nanoparticles might lead to a small perturbation in the surface and/or electronic structure of titania that results in an overabundance of relatively electron-rich terminal hydroxyl groups directly at the MSI.

# CONCLUSIONS

The spectroscopic results during  $H_2$  adsorption indicate intimate local electronic interactions between the catalyst components, whereby electron density is transferred from Au to  $TiO_2$ . The experimental ratio of approximately one active hydroxyl per  $Au_{per}$  atom suggests that this electronic

modification coincides with a structural modification of the support at the interface. These synergistic structural and electronic interactions appear to facilitate heterolytic  $\rm H_2$  activation (relative to pure Au surfaces). The electron transfer from Au to  $\rm TiO_2$  makes the Au surface somewhat electron poor, which facilitates the stabilization of a developing hydride. This interaction also increases the electron richness of MSI hydroxyls, making them more basic and more able to stabilize the developing proton.

### ASSOCIATED CONTENT

# **Solution** Supporting Information

The Supporting Information is available free of charge at https://pubs.acs.org/doi/10.1021/acscatal.1c04419.

Experimental section; materials and methods; STEM characterization; particle size analysis; sample pretreatment before FTIR experiments; representative FTIR spectra; choice of spectral range for BBA analysis; BBA $_{\rm P,T}$  extraction from BBA profiles; BBA calibration using volumetric  $\rm H_2$  adsorption; titration of MSI sites; and the extracted peak areas of  $_{\rm MSI}$ TiOH and  $_{\rm MSI}$ TiOH $_2^+$  (stretching and scissoring) as a function of the number of active perimeter sites determined using FTIR titration and STEM image analysis (PDF)

### AUTHOR INFORMATION

# **Corresponding Author**

Bert D. Chandler — Department of Chemistry, Trinity University, San Antonio, Texas 78212-7200, United States; Department of Chemical Engineering, The Pennsylvania State University, University Park, Pennsylvania 16802, United States; Department of Chemistry, The Pennsylvania State University, University Park, Pennsylvania 16802, United States; orcid.org/0000-0002-8621-0361; Phone: (814) 863-6229; Email: bert.chandler@psu.edu

### **Authors**

Akbar Mahdavi-Shakib — Department of Chemistry, Trinity University, San Antonio, Texas 78212-7200, United States; Department of Chemistry, The Pennsylvania State University, University Park, Pennsylvania 16802, United States

Lauren C. Rich – Department of Chemistry, Trinity University, San Antonio, Texas 78212-7200, United States

Todd N. Whittaker – Department of Chemistry, Trinity University, San Antonio, Texas 78212-7200, United States; Department of Chemical and Biological Engineering, The University of Colorado, Boulder, Colorado 80303, United States

Complete contact information is available at: https://pubs.acs.org/10.1021/acscatal.1c04419

# Notes

The authors declare no competing financial interest.

### ACKNOWLEDGMENTS

The authors gratefully acknowledge the National Science Foundation (Awards CBET-1803769, CBET-1803808, and CHE-1566301) and the Research Corporation for Science Advancement for supporting this work. The authors thank Tianze Xie and Prof. Robert M. Rioux at the Pennsylvania State University for their assistance in collecting TEM data.

### REFERENCES

- (1) Ponec, V.; Bond, G. C. *Catalysis by Metals and Alloys*; Studies in Surface Science and Catalysis; Elsevier: Amsterdam, 1995; Vol. 95, pp 1–744.
- (2) Greeley, J. P. Active Site of an Industrial Catalyst. *Science* **2012**, 336, 810–811.
- (3) Behrens, M.; Felix, S.; Igor, K.; Stefanie, K.; Michael, H.; Frank, A.-P.; Stefan, Z.; Frank, G.; Patrick, K.; Benjamin-Louis, K.; Michael, T.; Fischer, R. W.; Nørskov, J. K.; Robert, S. The Active Site of Methanol Synthesis over Cu/ZnO/Al<sub>2</sub>O<sub>3</sub> Industrial Catalysts. *Science* **2012**, 336, 893–897.
- (4) Daage, M.; Chianelli, R. R. Structure-Function Relations in Molybdenum Sulfide Catalysts: The "Rim-Edge" Model. *J. Catal.* **1994**, *149*, 414–427.
- (5) Chen, M.; Dheeraj, K.; Cheol-Woo, Y.; Wayne, G. D. The Promotional Effect of Gold in Catalysis by Palladium-Gold. *Science* **2005**, *310*, 291–293.
- (6) Kattel, S.; Yan, B.; Yang, Y.; Chen, J. G.; Liu, P. Optimizing Binding Energies of Key Intermediates for CO<sub>2</sub> Hydrogenation to Methanol over Oxide-Supported Copper. *J. Am. Chem. Soc.* **2016**, *138*, 12440–12450.
- (7) Kattel, S.; Ramírez, P. J.; Chen, J. G.; Rodriguez, J. A.; Ping, L. Active Sites for CO<sub>2</sub> Hydrogenation to Methanol on Cu/ZnO Catalysts. *Science* **2017**, 355, 1296–1299.
- (8) Lam, E.; Corral-Pérez, J. J.; Larmier, K.; Noh, G.; Wolf, P.; Comas-Vives, A.; Urakawa, A.; Copéret, C. CO<sub>2</sub> Hydrogenation on Cu/Al<sub>2</sub>O<sub>3</sub>: Role of the Metal/Support Interface in Driving Activity and Selectivity of a Bifunctional Catalyst. *Angew. Chem., Int. Ed.* **2019**, 58, 13989–13996.
- (9) Larmier, K.; Liao, W.-C.; Tada, S.; Lam, E.; Verel, R.; Bansode, A.; Urakawa, A.; Comas-Vives, A.; Copéret, C. CO<sub>2</sub>-to-Methanol Hydrogenation on Zirconia-Supported Copper Nanoparticles: Reaction Intermediates and the Role of the Metal—Support Interface. *Angew. Chem., Int. Ed.* **2017**, *56*, 2318–2323.
- (10) Robinson, A. M.; Hensley, J. E.; Medlin, J. W. Bifunctional Catalysts for Upgrading of Biomass-Derived Oxygenates: A Review. ACS Catal. 2016, 6, 5026–5043.
- (11) Saavedra, J.; Doan, H. A.; Pursell, C. J.; Grabow, L. C.; Chandler, B. D. The Critical Role of Water at the Gold-Titania Interface in Catalytic CO Oxidation. *Science* **2014**, 345, 1599–1602.
- (12) Wang, Y.; Widmann, D.; Heenemann, M.; Diemant, T.; Biskupek, J.; Schlögl, R.; Behm, R. J. The Role of Electronic Metal-Support Interactions and Its Temperature Dependence: CO Adsorption and CO Oxidation on Au/TiO<sub>2</sub> Catalysts in the Presence of TiO<sub>2</sub> Bulk Defects. *J. Catal.* **2017**, *354*, 46–60.
- (13) Green, I. X.; Wenjie, T.; Matthew, N.; Yates, J. T. Spectroscopic Observation of Dual Catalytic Sites During Oxidation of CO on a Au/TiO<sub>2</sub> Catalyst. *Science* **2011**, 333, 736–739.
- (14) Carrasquillo-Flores, R.; Ro, I.; Kumbhalkar, M. D.; Burt, S.; Carrero, C. A.; Alba-Rubio, A. C.; Miller, J. T.; Hermans, I.; Huber, G. W.; Dumesic, J. A. Reverse Water—Gas Shift on Interfacial Sites Formed by Deposition of Oxidized Molybdenum Moieties onto Gold Nanoparticles. *J. Am. Chem. Soc.* **2015**, *137*, 10317—10325.
- (15) Zhao, Z.-J.; Li, Z.; Cui, Y.; Zhu, H.; Schneider, W. F.; Delgass, W. N.; Ribeiro, F.; Greeley, J. Importance of Metal-Oxide Interfaces in Heterogeneous Catalysis: A Combined DFT, Microkinetic, and Experimental Study of Water-Gas Shift on Au/MgO. *J. Catal.* **2017**, 345, 157–169.
- (16) Wang, L.; Zhang, J.; Wang, H.; Shao, Y.; Liu, X.; Wang, Y.-Q.; Lewis, J. P.; Xiao, F.-S. Activity and Selectivity in Nitroarene Hydrogenation over Au Nanoparticles on the Edge/Corner of Anatase. *ACS Catal.* **2016**, *6*, 4110–4116.
- (17) Corma, A.; Pedro, S. Chemoselective Hydrogenation of Nitro Compounds with Supported Gold Catalysts. *Science* **2006**, *313*, 332–334.
- (18) Zhu, Y. P.; Guo, C.; Zheng, Y.; Qiao, S.-Z. Surface and Interface Engineering of Noble-Metal-Free Electrocatalysts for Efficient Energy Conversion Processes. *Acc. Chem. Res.* **2017**, *50*, 915–923.

- (19) Song, F.; Li, W.; Yang, J.; Han, G.; Yan, T.; Liu, X.; Rao, Y.; Liao, P.; Cao, Z.; Sun, Y. Interfacial Sites between Cobalt Nitride and Cobalt Act as Bifunctional Catalysts for Hydrogen Electrochemistry. *ACS Energy Lett.* **2019**, *4*, 1594–1601.
- (20) Bamwenda, G. R.; Tsubota, S.; Nakamura, T.; Haruta, M. The Influence of the Preparation Methods on the Catalytic Activity of Platinum and Gold Supported on TiO<sub>2</sub> for CO Oxidation. *Catal. Lett.* **1997**, *44*, 83–87.
- (21) Ide, M. S.; Davis, R. J. The Important Role of Hydroxyl on Oxidation Catalysis by Gold Nanoparticles. *Acc. Chem. Res.* **2014**, *47*, 825–833.
- (22) Pina, C.; della Falletta, E.; Rossi, M. Update on Selective Oxidation Using Gold. Chem. Soc. Rev. 2012, 41, 350–369.
- (23) Corma, A.; Garcia, H. Supported Gold Nanoparticles as Catalysts for Organic Reactions. *Chem. Soc. Rev.* **2008**, 37, 2096–2126.
- (24) Turner, M.; Golovko, V. B.; Vaughan, O. P. H.; Abdulkin, P.; Berenguer-Murcia, A.; Tikhov, M. S.; Johnson, B. F. G.; Lambert, R. M. Selective Oxidation with Dioxygen by Gold Nanoparticle Catalysts Derived from 55-Atom Clusters. *Nature* **2008**, *454*, 981–983.
- (25) Xu, B.; Madix, R. J.; Friend, C. M. Predicting Gold-Mediated Catalytic Oxidative-Coupling Reactions from Single Crystal Studies. *Acc. Chem. Res.* **2014**, *47*, 761–772.
- (26) Grirrane, A.; Avelino, C.; Hermenegildo, G. Gold-Catalyzed Synthesis of Aromatic Azo Compounds from Anilines and Nitroaromatics. *Science* **2008**, 322, 1661–1664.
- (27) Stratakis, M.; Garcia, H. Catalysis by Supported Gold Nanoparticles: Beyond Aerobic Oxidative Processes. *Chem. Rev.* **2012**, *112*, 4469–4506.
- (28) Sankar, M.; He, Q.; Engel, Rv.; Sainna, M. A.; Logsdail, A. J.; Roldan, A.; Willock, D. J.; Agarwal, N.; Kiely, C. J.; Hutchings, G. J. Role of the Support in Gold-Containing Nanoparticles as Heterogeneous Catalysts. *Chem. Rev.* **2020**, *120*, 3890–3938.
- (29) Widmann, D.; Behm, R. J. Activation of Molecular Oxygen and the Nature of the Active Oxygen Species for CO Oxidation on Oxide Supported Au Catalysts. *Acc. Chem. Res.* **2014**, *47*, 740–749.
- (30) Pan, M.; Gong, J.; Dong, G.; Mullins, C. B. Model Studies with Gold: A Versatile Oxidation and Hydrogenation Catalyst. *Acc. Chem. Res.* **2014**, 47, 750–760.
- (31) Green, I. X.; Tang, W.; Neurock, M.; Yates, J. T. Insights into Catalytic Oxidation at the Au/TiO<sub>2</sub> Dual Perimeter Sites. *Acc. Chem. Res.* **2014**, 47, 805–815.
- (32) Wu, Y. Y.; Mashayekhi, N. A.; Kung, H. H. Au-Metal Oxide Support Interface as Catalytic Active Sites. *Catal. Sci. Technol.* **2013**, 3, 2881–2891.
- (33) Adams, J. S.; Ashwin, C.; Pranjali, P.; Tomas, R.; Yubing, L.; Vineet, M.; Abinaya, S.; Stuart, W.; M, K. A.; Matthew, N.; Flaherty, D. W. Solvent Molecules Form Surface Redox Mediators in Situ and Cocatalyze O2 Reduction on Pd. Science 2021, 371, 626–632.
- (34) Zope, B. N.; Hibbitts, D. D.; Neurock, M.; Davis, R. J. Reactivity of the Gold/Water Interface During Selective Oxidation Catalysis. *Science* **2010**, 330, 74–78.
- (35) Siporin, S. E.; Davis, R. J. Use of Kinetic Models to Explore the Role of Base Promoters on Ru/MgO Ammonia Synthesis Catalysts. *J. Catal.* **2004**, 225, 359–368.
- (36) Masoud, N.; Delannoy, L.; Schaink, H.; van der Eerden, A.; de Rijk, J. W.; Silva, T. A. G.; Banerjee, D.; Meeldijk, J. D.; de Jong, K. P.; Louis, C.; de Jongh, P. E. Superior Stability of Au/SiO2 Compared to Au/TiO<sub>2</sub> Catalysts for the Selective Hydrogenation of Butadiene. *ACS Catal.* **2017**, *7*, 5594–5603.
- (37) Aguilar-Tapia, A.; Delannoy, L.; Louis, C.; Han, C. W.; Ortalan, V.; Zanella, R. Selective Hydrogenation of 1,3-Butadiene over Bimetallic Au-Ni/TiO<sub>2</sub> Catalysts Prepared by Deposition-Precipitation with Urea. *J. Catal.* **2016**, 344, 515–523.
- (38) Bruno, J. E.; Sravan Kumar, K. B.; Dwarica, N. S.; Hüther, A.; Chen, Z.; Guzman, C. S., IV; Hand, E. R.; Moore, W. C.; Rioux, R. M.; Grabow, L. C.; Chandler, B. D. On the Limited Role of Electronic Support Effects in Selective Alkyne Hydrogenation: A Kinetic Study

- of Au/MOx Catalysts Prepared from Oleylamine-Capped Colloidal Nanoparticles. *ChemCatChem* **2019**, *11*, 1650–1664.
- (39) Fiorio, J. L.; Gonçalves, R. V.; Teixeira-Neto, E.; Ortuño, M. A.; López, N.; Rossi, L. M. Accessing Frustrated Lewis Pair Chemistry through Robust Gold@N-Doped Carbon for Selective Hydrogenation of Alkynes. *ACS Catal.* **2018**, *8*, 3516–3524.
- (40) Fiorio, J. L.; López, N.; Rossi, L. M. Gold-Ligand-Catalyzed Selective Hydrogenation of Alkynes into Cis-Alkenes via H<sub>2</sub> Heterolytic Activation by Frustrated Lewis Pairs. *ACS Catal.* **2017**, 7, 2973–2980.
- (41) Hugon, A.; Delannoy, L.; Krafft, J.-M.; Louis, C. Selective Hydrogenation of 1,3-Butadiene in the Presence of an Excess of Alkenes over Supported Bimetallic Gold—Palladium Catalysts. *J. Phys. Chem. C* **2010**, *114*, 10823—10835.
- (42) Lopez-Sanchez, J. A.; Lennon, D. The Use of Titania- and Iron Oxide-Supported Gold Catalysts for the Hydrogenation of Propyne. *Appl. Catal.*, A **2005**, 291, 230–237.
- (43) Gluhoi, A. C.; Bakker, J. W.; Nieuwenhuys, B. E. Gold, Still a Surprising Catalyst: Selective Hydrogenation of Acetylene to Ethylene over Au Nanoparticles. *Catal. Today* **2010**, *154*, 13–20.
- (44) Zanella, R.; Louis, C.; Giorgio, S.; Touroude, R. Crotonaldehyde Hydrogenation by Gold Supported on TiO<sub>2</sub>: Structure Sensitivity and Mechanism. *J. Catal.* **2004**, 223, 328–339.
- (45) Stephenson, C. J.; Whitford, C. L.; Stair, P. C.; Farha, O. K.; Hupp, J. T. Chemoselective Hydrogenation of Crotonaldehyde Catalyzed by an Au@ZIF-8 Composite. *ChemCatChem* **2016**, *8*, 855–860.
- (46) Serna, P.; Boronat, M.; Corma, A. Tuning the Behavior of Au and Pt Catalysts for the Chemoselective Hydrogenation of Nitroaromatic Compounds. *Top. Catal.* **2011**, *54*, 439–446.
- (47) Corma, A.; Serna, P.; García, H. Gold Catalysts Open a New General Chemoselective Route to Synthesize Oximes by Hydrogenation of  $\alpha,\beta$ -Unsaturated Nitrocompounds with H2. *J. Am. Chem. Soc.* **2007**, *129*, 6358–6359.
- (48) Yuan, G.; Lopez, J. L.; Louis, C.; Delannoy, L.; Keane, M. A. Remarkable Hydrodechlorination Activity over Silica Supported Nickel/Gold Catalysts. *Catal. Commun.* **2005**, *6*, 555–562.
- (49) Ruiz, V. R.; Velty, A.; Santos, L. L.; Leyva-Pérez, A.; Sabater, M. J.; Iborra, S.; Corma, A. Gold Catalysts and Solid Catalysts for Biomass Transformations: Valorization of Glycerol and Glycerol—Water Mixtures through Formation of Cyclic Acetals. *J. Catal.* **2010**, 271, 351–357.
- (50) Masoud, N.; Donoeva, B.; de Jongh, P. E. Stability of Gold Nanocatalysts Supported on Mesoporous Silica for the Oxidation of S-Hydroxymethyl Furfural to Furan-2,5-Dicarboxylic Acid. *Appl. Catal., A* **2018**, *561*, 150–157.
- (51) Donoeva, B.; Masoud, N.; de Jongh, P. E. Carbon Support Surface Effects in the Gold-Catalyzed Oxidation of 5-Hydroxymethylfurfural. *ACS Catal.* **2017**, *7*, 4581–4591.
- (52) Casanova, O.; Iborra, S.; Corma, A. Biomass into Chemicals: One Pot-Base Free Oxidative Esterification of 5-Hydroxymethyl-2-Furfural into 2,5-Dimethylfuroate with Gold on Nanoparticulated Ceria. *J. Catal.* **2009**, 265, 109–116.
- (53) Juárez, R.; Parker, S. F.; Concepción, P.; Corma, A.; García, H. Heterolytic and Heterotopic Dissociation of Hydrogen on Ceria-Supported Gold Nanoparticles. Combined Inelastic Neutron Scattering and FT-IR Spectroscopic Study on the Nature and Reactivity of Surface Hydrogen Species. *Chem. Sci.* **2010**, *1*, 731–738.
- (54) Sravan Kumar, K. B.; Whittaker, T. N.; Peterson, C.; Grabow, L. C.; Chandler, B. D. Water Poisons H<sub>2</sub> Activation at the Au–TiO<sub>2</sub> Interface by Slowing Proton and Electron Transfer between Au and Titania. *J. Am. Chem. Soc.* **2020**, *142*, 5760–5772.
- (55) Bruno, J. E.; Dwarica, N. S.; Whittaker, T. N.; Hand, E. R.; Guzman, C. S.; Dasgupta, A.; Chen, Z.; Rioux, R. M.; Chandler, B. D. Supported Ni–Au Colloid Precursors for Active, Selective, and Stable Alkyne Partial Hydrogenation Catalysts. *ACS Catal.* **2020**, *10*, 2565–2580
- (56) Whittaker, T. N.; Sravan Kumar, K. B.; Peterson, C.; Pollock, M. N.; Grabow, L. C.; Chandler, B. D. H<sub>2</sub> Oxidation over Supported

- Au Nanoparticle Catalysts: Evidence for Heterolytic H<sub>2</sub> Activation at the Metal—Support Interface. *J. Am. Chem. Soc.* **2018**, *140*, 16469—16487.
- (57) Mahdavi-Shakib, A.; Sravan Kumar, K. B.; Whittaker, T. N.; Xie, T.; Grabow, L. C.; Rioux, R. M.; Chandler, B. D. Kinetics of H<sub>2</sub> Adsorption at the Metal—Support Interface of Au/TiO<sub>2</sub> Catalysts Probed by Broad Background IR Absorbance. *Angew. Chem., Int. Ed.* **2021**, *60*, 7735–7743.
- (58) Takei, T.; Akita, T.; Nakamura, I.; Fujitani, T.; Okumura, M.; Okazaki, K.; Huang, J.; Ishida, T.; Haruta, M. Chapter One Heterogeneous Catalysis by Gold. *Adv. Catal.* **2012**, *55*, 1–126.
- (59) Min, B. K.; Friend, C. M. Heterogeneous Gold-Based Catalysis for Green Chemistry: Low-Temperature CO Oxidation and Propene Oxidation. *Chem. Rev.* **2007**, *107*, 2709–2724.
- (60) Janssens, T. V. W.; Clausen, B. S.; Hvolbæk, B.; Falsig, H.; Christensen, C. H.; Bligaard, T.; Nørskov, J. K. Insights into the Reactivity of Supported Au Nanoparticles: Combining Theory and Experiments. *Top. Catal.* **2007**, *44*, 15.
- (61) Chen, M.; Goodman, D. W. Catalytically Active Gold: From Nanoparticles to Ultrathin Films. Acc. Chem. Res. 2006, 39, 739–746.
- (62) Ishida, T.; Murayama, T.; Taketoshi, A.; Haruta, M. Importance of Size and Contact Structure of Gold Nanoparticles for the Genesis of Unique Catalytic Processes. *Chem. Rev.* **2020**, *120*, 464–525.
- (63) Cargnello, M.; Doan-Nguyen, V. V. T.; Gordon, T. R.; Diaz, R. E.; Stach, E. A.; Gorte, R. J.; Fornasiero, P.; Murray, C. B. Control of Metal Nanocrystal Size Reveals Metal-Support Interface Role for Ceria Catalysts. *Science* **2013**, *341*, 771–773.
- (64) Green, I. X.; Tang, W.; Neurock, M.; Yates, J. T., Jr. Low-Temperature Catalytic H<sub>2</sub> Oxidation over Au Nanoparticle/TiO2 Dual Perimeter Sites. *Angew. Chem., Int. Ed.* **2011**, *50*, 10186–10189.
- (65) Panayotov, D. A.; Yates, J. T. Depletion of Conduction Band Electrons in TiO<sub>2</sub> by Water Chemisorption IR Spectroscopic Studies of the Independence of Ti–OH Frequencies on Electron Concentration. *Chem. Phys. Lett.* **2005**, 410, 11–17.
- (66) Panayotov, D. A.; Burrows, S. P.; Yates, J. T.; Morris, J. R. Mechanistic Studies of Hydrogen Dissociation and Spillover on Au/TiO<sub>2</sub>: IR Spectroscopy of Coadsorbed CO and H-Donated Electrons. *J. Phys. Chem. C* **2011**, *115*, 22400–22408.
- (67) Gibson, A. F. Infra-Red and Microwave Modulation Using Free Carriers in Semiconductors. *J. Sci. Instrum.* **1958**, *35*, 273–278.
- (68) Silverwood, I. P.; Rogers, S. M.; Callear, S. K.; Parker, S. F.; Catlow, C. R. A. Evidence for a Surface Gold Hydride on a Nanostructured Gold Catalyst. *Chem. Commun.* **2016**, *52*, 533–536.
- (69) Panayotov, D. A.; Burrows, S. P.; Morris, J. R. Photooxidation Mechanism of Methanol on Rutile TiO<sub>2</sub> Nanoparticles. *J. Phys. Chem.* C **2012**, *116*, 6623–6635.
- (70) Yuan, W.; Beien, Z.; Ke, F.; Xiao-Yan, L.; Hansen, T. W.; Yang, O.; Hangsheng, Y.; B, W. J.; Yi, G.; Yong, W.; Ze, Z. In Situ Manipulation of the Active Au-TiO<sub>2</sub> Interface with Atomic Precision during CO Oxidation. *Science* **2021**, *371*, 517–521.
- (71) Liu, P.; Arslan Irmak, E.; de Backer, A.; de wael, A.; Lobato, I.; Béché, A.; van Aert, S.; Bals, S. Three-Dimensional Atomic Structure of Supported Au Nanoparticles at High Temperature. *Nanoscale* **2021**, *13*, 1770–1776.
- (72) Delannoy, L.; Chantry, R. L.; Casale, S.; Li, Z. Y.; Borensztein, Y.; Louis, C. HRTEM and STEM-HAADF Characterisation of Au—TiO<sub>2</sub> and Au—Al<sub>2</sub>O<sub>3</sub> Catalysts for a Better Understanding of the Parameters Influencing Their Properties in CO Oxidation. *Phys. Chem. Chem. Phys.* **2013**, *15*, 3473—3479.
- (73) Mahdavi-Shakib, A.; Arce-Ramos, J. M.; Austin, R. N.; Schwartz, T. J.; Grabow, L. C.; Frederick, B. G. Frequencies and Thermal Stability of Isolated Surface Hydroxyls on Pyrogenic  ${\rm TiO_2}$  Nanoparticles. *J. Phys. Chem. C* **2019**, *123*, 24533–24548.
- (74) Arrouvel, C.; Digne, M.; Breysse, M.; Toulhoat, H.; Raybaud, P. Effects of Morphology on Surface Hydroxyl Concentration: A DFT Comparison of Anatase–TiO<sub>2</sub> and γ-Alumina Catalytic Supports. *J. Catal.* **2004**, 222, 152–166.

- (75) Wang, S.; Petzold, V.; Tripkovic, V.; Kleis, J.; Howalt, J. G.; Skúlason, E.; Fernández, E. M.; Hvolbæk, B.; Jones, G.; Toftelund, A.; Falsig, H.; Björketun, M.; Studt, F.; Abild-Pedersen, F.; Rossmeisl, J.; Nørskov, J. K.; Bligaard, T. Universal Transition State Scaling Relations for (de)Hydrogenation over Transition Metals. *Phys. Chem. Phys.* **2011**, *13*, 20760–20765.
- (76) Lyalin, A.; Taketsugu, T. A Computational Investigation of  $H_2$  Adsorption and Dissociation on Au Nanoparticles Supported on TiO2 Surface. Faraday Discuss. **2011**, 152, 185–201.
- (77) Boronat, M.; Illas, F.; Corma, A. Active Sites for  $H_2$  Adsorption and Activation in  $Au/TiO_2$  and the Role of the Support. *J. Phys. Chem.* A **2009**, 113, 3750–3757.
- (78) Corma, A.; Boronat, M.; González, S.; Illas, F. On the Activation of Molecular Hydrogen by Gold: A Theoretical Approximation to the Nature of Potential Active Sites. *Chem. Commun.* **2007**, 3371–3373.
- (79) Banerjee, S.; Zangiabadi, A.; Mahdavi-Shakib, A.; Husremovic, S.; Frederick, B. G.; Barmak, K.; Austin, R. N.; Billinge, S. J. L. Quantitative Structural Characterization of Catalytically Active TiO<sub>2</sub> Nanoparticles. *ACS Appl. Nano Mater.* **2019**, *2*, 6268–6276.
- (80) Fornaro, T.; Burini, D.; Biczysko, M.; Barone, V. Hydrogen-Bonding Effects on Infrared Spectra from Anharmonic Computations: Uracil—Water Complexes and Uracil Dimers. *J. Phys. Chem. A* **2015**, 119, 4224–4236.
- (81) Seki, T.; Sun, S.; Zhong, K.; Yu, C.-C.; Machel, K.; Dreier, L. B.; Backus, E. H. G.; Bonn, M.; Nagata, Y. Unveiling Heterogeneity of Interfacial Water through the Water Bending Mode. *J. Phys. Chem. Lett.* **2019**, *10*, 6936–6941.
- (82) Seki, T.; Chiang, K.-Y.; Yu, C.-C.; Yu, X.; Okuno, M.; Hunger, J.; Nagata, Y.; Bonn, M. The Bending Mode of Water: A Powerful Probe for Hydrogen Bond Structure of Aqueous Systems. *J. Phys. Chem. Lett.* **2020**, *11*, 8459–8469.
- (83) Yan, C.; Xue, Z.; Zhao, W.; Wang, J.; Mu, T. Surprising Hofmeister Effects on the Bending Vibration of Water. *ChemPhysChem* **2016**, *17*, 3309–3314.
- (84) Ojha, D.; Henao, A.; Kühne, T. D. Nuclear Quantum Effects on the Vibrational Dynamics of Liquid Water. *J. Chem. Phys.* **2017**, *148*, No. 102328.
- (85) Falk, M. The Frequency of the H-O-H Bending Fundamental in Solids and Liquids. *Spectrochim. Acta, Part A* **1984**, *40*, 43–48.
- (86) Bond, G. C.; Thompson, D. T. Catalysis by Gold. Catal. Rev. 1999, 41, 319-388.
- (87) Fujitani, T.; Nakamura, I.; Takahashi, A. H<sub>2</sub>O Dissociation at the Perimeter Interface between Gold Nanoparticles and TiO<sub>2</sub> Is Crucial for Oxidation of CO. ACS Catal. **2020**, 10, 2517–2521.
- (88) Saavedra, J.; Whittaker, T.; Chen, Z.; Pursell, C. J.; Rioux, R. M.; Chandler, B. D. Controlling Activity and Selectivity Using Water in the Au-Catalysed Preferential Oxidation of CO in H<sub>2</sub>. *Nat. Chem.* **2016**, *8*, 584–589.
- (89) Bowker, M. The Surface Structure of Titania and the Effect of Reduction. *Curr. Opin. Solid State Mater. Sci.* **2006**, *10*, 153–162.
- (90) Diebold, U. Structure and Properties of TiO<sub>2</sub> Surfaces: A Brief Review. Appl. Phys. A: Mater. Sci. Process. 2003, 76, 681–687.

### ■ NOTE ADDED AFTER ASAP PUBLICATION

This paper published ASAP on Dec 7, 2021 with a production error in the first author's name. The mistake was corrected and the revised paper reposted on Dec 8, 2021.